



# Enhanced light-matter interactions in graphene-covered dielectric magnetic mirrors

YIPING LIU,<sup>1</sup> YUNYUN DAI,<sup>2</sup> QIANCHI FENG,<sup>2</sup> YUWEI SHAN,<sup>2</sup> LEI DU,<sup>1</sup> YUYU XIA,<sup>2</sup> GUANG LU,<sup>1</sup> FEN LIU,<sup>1</sup> GUIQIANG DU,<sup>1,2,\*</sup> CHUANSHAN TIAN,<sup>2</sup> SHIWEI WU,<sup>2</sup> LEI SHI,<sup>2</sup> AND JIAN ZI<sup>2</sup>

<sup>1</sup>*School of Space Science and Physics, Shandong University at Weihai, Weihai 264209, China*

<sup>2</sup>*State Key Laboratory of Surface Physics and Department of Physics, Key Laboratory of Micro- and Nano-Photonic Structures (Ministry of Education), Fudan University, Shanghai 200433, China*

\*[dgqql@sdu.edu.cn](mailto:dgqql@sdu.edu.cn)

**Abstract:** Enhanced interactions of light with graphene on the surface of a lossless dielectric magnetic mirror (DMM) are studied theoretically and experimentally in the visible range, where the DMM is composed of truncated dielectric photonic crystals (PCs). The absorption of graphene on the DMM was enhanced by about 4-fold for the spectral range within the forbidden gap of PCs over a wide range of incidence angles for both transverse electric and transverse magnetic polarizations compared with that of free-standing graphene. Moreover, the enhanced local electric field on the DMM surface led to much better detection efficiencies of the photocurrent, Raman spectroscopy and enhanced third-harmonic generation of graphene. These results offer a new way to achieve an enhanced interaction of light with graphene and develop new compact graphene-based devices.

© 2017 Optical Society of America under the terms of the [OSA Open Access Publishing Agreement](#)

**OCIS codes:** (230.5298) Photonic crystals; (310.3915) Metallic, opaque, and absorbing coatings; (240.4350) Nonlinear optics at surfaces; (190.2620) Harmonic generation and mixing.

## References and links

1. K. S. Novoselov, A. K. Geim, S. V. Morozov, D. Jiang, M. I. Katsnelson, I. V. Grigorieva, S. V. Dubonos, and A. A. Firsov, "Two-dimensional gas of massless Dirac fermions in graphene," *Nature* **438**(7065), 197–200 (2005).
2. S. Bae, H. Kim, Y. Lee, X. Xu, J. S. Park, Y. Zheng, J. Balakrishnan, T. Lei, H. R. Kim, Y. I. Song, Y. J. Kim, K. S. Kim, B. Özyilmaz, J. H. Ahn, B. H. Hong, and S. Iijima, "Roll-to-roll production of 30-inch graphene films for transparent electrodes," *Nat. Nanotechnol.* **5**(8), 574–578 (2010).
3. W. D. Tan, C. Y. Su, R. J. Knize, G. Q. Xie, L. J. Li, and D. Y. Tang, "Mode locking of ceramic Nd:yttrium aluminum garnet with graphene as a saturable absorber," *Appl. Phys. Lett.* **96**(3), 031106 (2010).
4. Q. L. Bao, H. Zhang, B. Wang, Z. H. Ni, C. H. Y. X. Lim, Y. Wang, D. Y. Tang, and K. P. Loh, "Broadband graphene polarizer," *Nat. Photonics* **5**, 411–415 (2011).
5. Z. Fang, Z. Liu, Y. Wang, P. M. Ajayan, P. Nordlander, and N. J. Halas, "Graphene-Antenna Sandwich Photodetector," *Nano Lett.* **12**(7), 3808–3813 (2012).
6. L. Gao, W. Ren, B. Liu, R. Saito, Z. S. Wu, S. Li, C. Jiang, F. Li, and H. M. Cheng, "Surface and Interference Coenhanced Raman Scattering of Graphene," *ACS Nano* **3**(4), 933–939 (2009).
7. W. Xu, X. Ling, J. Xiao, M. S. Dresselhaus, J. Kong, H. Xu, Z. Liu, and J. Zhang, "Surface enhanced Raman spectroscopy on a flat graphene surface," *Proc. Natl. Acad. Sci. U.S.A.* **109**(24), 9281–9286 (2012).
8. H. K. Baghbadorani, J. Barvestani, and S. R. Entezar, "Biosensors based on Bloch surface waves in one-dimensional photonic crystal with graphene nanolayers," *Appl. Opt.* **56**(3), 462–469 (2017).
9. I. Degli-Eredi, J. E. Sipe, and N. Vermeulen, "TE-polarized graphene modes sustained by photonic crystal structures," *Opt. Lett.* **40**(9), 2076–2079 (2015).
10. K. Kim, S. H. Cho, and C. W. Lee, "Nonlinear optics: Graphene-silicon fusion," *Nat. Photonics* **6**, 502–503 (2012).
11. H. Zhang, S. Virally, Q. Bao, L. K. Ping, S. Massar, N. Godbout, and P. Kockaert, "Z-scan measurement of the nonlinear refractive index of graphene," *Opt. Lett.* **37**(11), 1856–1858 (2012).
12. M. Gullans, D. E. Chang, F. H. L. Koppens, F. J. García de Abajo, and M. D. Lukin, "Single-Photon Nonlinear Optics with Graphene Plasmons," *Phys. Rev. Lett.* **111**(24), 247401 (2013).
13. S. Y. Hong, J. I. Dadap, N. Petrone, P. C. Yeh, J. Hone, and R. M. Osgood, Jr., "Optical Third-Harmonic Generation in Graphene," *Phys. Rev. X* **3**(2), 021014 (2013).
14. N. Kumar, J. Kumar, C. Gerstenkorn, R. Wang, H. Y. Chiu, A. L. Smirl, and H. Zhao, "Third harmonic generation in graphene and few-layer graphite films," *Phys. Rev. B* **87**(12), 121406 (2013).

15. R. R. Nair, P. Blake, A. N. Grigorenko, K. S. Novoselov, T. J. Booth, T. Stauber, N. M. R. Peres, and A. K. Geim, "Fine Structure Constant Defines Visual Transparency of Graphene," *Science* **320**(5881), 1308 (2008).
16. F. Xia, T. Mueller, Y. M. Lin, A. Valdes-Garcia, and P. Avouris, "Ultrafast graphene photodetector," *Nat. Nanotechnol.* **4**(12), 839–843 (2009).
17. M. Furchi, A. Urich, A. Pospischil, G. Lilley, K. Unterrainer, H. Detz, P. Klang, A. M. Andrews, W. Schrenk, G. Strasser, and T. Mueller, "Microcavity-Integrated Graphene Photodetector," *Nano Lett.* **12**(6), 2773–2777 (2012).
18. S. Thongrattanasiri, F. H. L. Koppens, and F. J. García de Abajo, "Complete Optical Absorption in Periodically Patterned Graphene," *Phys. Rev. Lett.* **108**(4), 047401 (2012).
19. G. Pirruccio, L. Martín Moreno, G. Lozano, and J. Gómez Rivas, "Coherent and Broadband Enhanced Optical Absorption in Graphene," *ACS Nano* **7**(6), 4810–4817 (2013).
20. J. R. Piper and S. Fan, "Total Absorption in a Graphene Monolayer in the Optical Regime by Critical Coupling with a Photonic Crystal Guided Resonance," *ACS Photonics* **1**(4), 347–353 (2014).
21. Z. Fang, Y. Wang, A. E. Schlather, Z. Liu, P. M. Ajayan, F. J. de Abajo, P. Nordlander, X. Zhu, and N. J. Halas, "Active Tunable Absorption Enhancement with Graphene Nanodisk Arrays," *Nano Lett.* **14**(1), 299–304 (2014).
22. T. J. Echtermeyer, L. Britnell, P. K. Jasnós, A. Lombardo, R. V. Gorbachev, A. N. Grigorenko, A. K. Geim, A. C. Ferrari, and K. S. Novoselov, "Strong plasmonic enhancement of photovoltage in graphene," *Nat. Commun.* **2**, 458 (2011).
23. X. Zhu, L. Shi, M. S. Schmidt, A. Boisen, O. Hansen, J. Zi, S. Xiao, and N. A. Mortensen, "Enhanced Light-Matter Interactions in Graphene-Covered Gold Nanovoid Arrays," *Nano Lett.* **13**(10), 4690–4696 (2013).
24. A. Ferreira, N. M. R. Peres, R. M. Ribeiro, and T. Stauber, "Graphene-based photodetector with two cavities," *Phys. Rev. B* **85**(11), 15438 (2012).
25. X. Gan, K. F. Mak, Y. Gao, Y. You, F. Hatami, J. Hone, T. F. Heinz, and D. Englund, "Strong enhancement of Light-Matter Interaction in Graphene Coupled to a Photonic Crystal Nanocavity," *Nano Lett.* **12**(11), 5626–5631 (2012).
26. A. S. Schwanecke, V. A. Fedotov, V. V. Khardikov, S. L. Prosvirnin, Y. Chen, and N. I. Zheludev, "Optical magnetic mirrors," *J. Opt. A, Pure Appl. Opt.* **9**(1), L1–L2 (2007).
27. M. Esfandyarpour, E. C. Garnett, Y. Cui, M. D. McGehee, and M. L. Brongersma, "Metamaterial mirrors in optoelectronic devices," *Nat. Nanotechnol.* **9**(7), 542–547 (2014).
28. J. C. Ginn, I. Brener, D. W. Peters, J. R. Wendt, J. O. Stevens, P. F. Hines, L. I. Basilio, L. K. Warne, J. F. Ihlefeld, P. G. Clem, and M. B. Sinclair, "Realizing optical magnetism from dielectric metamaterials," *Phys. Rev. Lett.* **108**(9), 097402 (2012).
29. L. Shi, T. U. Tuzer, R. Fenollosa, and F. Meseguer, "A new dielectric metamaterial building block with a strong magnetic response in the sub-1.5-micrometer region: silicon colloid nanocavities," *Adv. Mater.* **24**(44), 5934–5938 (2012).
30. S. Liu, M. B. Sinclair, T. S. Mahony, Y. C. Jun, S. Campione, J. Ginn, D. A. Bender, J. R. Wendt, J. F. Ihlefeld, P. G. Clem, J. B. Wright, and I. Brener, "Optical magnetic mirrors without metals," *Optica* **1**(4), 250–256 (2014).
31. A. Alù and N. Engheta, "Pairing an Epsilon-Negative Slab With a Mu-Negative Slab: Resonance, Tunneling and Transparency," *IEEE Trans. Antenn. Propag.* **51**(10), 2558–2571 (2003).
32. J. Guó, Y. Sun, Y. Zhang, H. Li, H. Jiang, and H. Chen, "Experimental investigation of interface states in photonic crystal heterostructures," *Phys. Rev. E Stat. Nonlin. Soft Matter Phys.* **78**(2 Pt 2), 026607 (2008).
33. J. C. Manifacier, J. Gasiot, and J. P. Fillard, "A simple method for the determination of the optical constants  $n$ ,  $k$  and the thickness of a weakly absorbing thin film," *J. Phys. Educ.* **9**(11), 1002–1004 (1976).
34. M. Bruna and S. Borini, "Optical constants of graphene layers in the visible range," *Appl. Phys. Lett.* **94**(3), 031901 (2009).
35. P. Yeh, *Optical Waves in Layered Media* (Wiley, 1988).
36. J. H. Apfel, "Graphical method to design multilayer phase retarders," *Appl. Opt.* **20**(6), 1024–1029 (1981).
37. J. H. Apfel, "Phase retardance of periodic multilayer mirrors," *Appl. Opt.* **21**(4), 733–738 (1982).
38. J. Wang, Y. Hernandez, M. Lotya, J. N. Coleman, and W. J. Blau, "Broadband Nonlinear Optical Response of Graphene Dispersions," *Adv. Mater.* **21**, 2430–2435 (2009).
39. A. Delfan, M. Liscidini, and J. E. Sipe, "Surface Enhanced Raman Scattering in the Presence of Multilayer Dielectric Structures," *J. Opt. Soc. Am. B* **29**(8), 1863–1874 (2012).
40. A. C. Ferrari and D. M. Basko, "Raman spectroscopy as a versatile tool for studying the properties of graphene," *Nat. Nanotechnol.* **8**(4), 235–246 (2013).
41. H. Budde, N. Coca-López, X. Shi, R. Ciesielski, A. Lombardo, D. Yoon, A. C. Ferrari, and A. Hartschuh, "Raman Radiation Patterns of Graphene," *ACS Nano* **10**(2), 1756–1763 (2016).
42. W. T. Liu, S. W. Wu, P. J. Schuck, M. Salmeron, Y. R. Shen, and F. Wang, "Nonlinear broadband photoluminescence of graphene induced by femtosecond laser irradiation," *Phys. Rev. B* **82**(8), 081408 (2010).

## 1. Introduction

Graphene has attracted considerable interest as an ultra-thin, two-dimensional material [1] because of its unique electrical and optical properties. These properties have led to numerous important applications in optoelectronic and nanophotonic devices, such as transparent

electrodes [2], ultrafast lasers [3], polarizers [4], detectors [5–7], sensors [8, 9], and nonlinear optical devices [10–14]. It is widely known that the absorption of graphene is approximately 2.3% over a broad wavelength range [15]. Although this absorptance value is considered to be very high with respect to the thickness of graphene, the absolute absorptance is still small, which limits its applications in optoelectronic devices that require stronger light-graphene interactions, such as graphene-based photodetectors [5, 16, 17] and optical absorbers [18–20]. Several methods have been proposed to enhance the absorption of graphene, including using patterned graphene [18, 21], combining graphene with conventional plasmonic nanostructures [22, 23], and integrating graphene with Fabry-Pérot microcavities [15, 24, 25]. Most of these approaches are suitable for specific wavelengths or a narrowband region. Specifically, for enhanced absorption by metallic plasmonic structures [22, 23], it is difficult to evaluate the pure graphene absorption due to the intrinsic absorption of the metal. When using Fabry-Pérot microcavities, the graphene layer is embedded inside the designed structure, resulting in difficulties in achieving further applications such as sensors and optoelectronic devices. Therefore, different approaches are highly desired to facilitate applications that meet the following requirements: 1) a wideband enhanced absorption of graphene, 2) an assisted structure composed of non-absorbing materials and 3) one surface of graphene that is exposed to the environmental medium. One of the most direct strategies to achieve these requirements is to use a perfect magnetic mirror [26–30] underneath the graphene layer to enhance the light-graphene interactions. However, metallic magnetic mirrors [26, 27] suffered from high intrinsic ohmic losses in the visible and infrared ranges, so all-dielectric nanostructures could be used to fabricate the perfect magnetic mirror [28–30].

Different from magnetic mirrors using two- or three-dimensional metamaterials [28–30], we proposed a dielectric magnetic mirror (DMM) based on a one-dimensional truncated all-dielectric photonic crystal (PC) to enhance the light-graphene interactions, where the graphene is covered on the surface of the DMM. Mirrors include magnetic mirrors and electric mirrors (such as a metallic mirror). In contrast to a perfect electric mirror, in which the reflection phase at its surface is  $\pi$ , the reflection phase equals 0 at the surface of the perfect magnetic mirror. However, because of the  $\pi$  phase shift of the reflected light in the case of a normal electric mirror, the electric fields of the incident light and the reflected light at the surface of the mirror are out of phase and cancel each other out, resulting in absorption properties of the graphene layer that are highly influenced by the distance between the graphene and the mirror. To ensure that the incident light and the reflected light are in phase at the mirror surface, a zero reflection phase shift is necessary. In this case, in contrast to the normal electric mirror, which is similar to epsilon-negative materials whose permittivity is negative, the mirror has a zero reflection phase, which is similar to mu-negative materials whose permeability is negative; thus, it can be called a magnetic mirror [26–32]. In this study, to realize a perfect magnetic mirror with a wide bandwidth that is composed of all-dielectric non-absorbing materials, one-dimensional dielectric PCs were designed and fabricated. With careful adjustment of the filling fraction of the PCs, the first-order photonic band gap exhibited perfect magnetic mirror behavior, leading to the enhanced wideband absorption of graphene on top of the PC, as demonstrated experimentally. Moreover, Cr/Au electrodes (source and drain) were deposited on the graphene layer to measure the photocurrents. Enhanced photocurrents were achieved by comparing the structures with monolayer graphene on the DMM and transparent substrates. Strong enhancements in the Raman spectrum and third-harmonic generation (THG) of graphene were also observed, which is essential for many optoelectronic applications.

## 2. Results and discussion

### 2.1 Enhanced absorption of graphene on the surface of the DMM

The DMM in this study is a one-dimensional truncated PC composed of alternating SiO<sub>2</sub> and TiO<sub>2</sub> layers. The graphene films are on the surface of the PC. The composite structure is

denoted as  $G(AB)^N AS$ , as shown in Fig. 1(a), where G represents the graphene, A denotes  $\text{SiO}_2$  with refractive index of  $n_A = 1.431$  [33] and a thickness of  $d_A = 98.5$  nm, B represents  $\text{TiO}_2$  with  $n_B = 2.123$  [33] and  $d_B = 66.4$  nm, N is the periodic number, and S is the substrate BK7 with  $n_S = 1.52$ . The refractive index of graphene is described by a simple model,  $n_G = 3.0 + C_1 \lambda i / 3$  ( $C_1 = 5.446 \mu\text{m}^{-1}$ ), in the visible range [34]. The thickness of a graphene monolayer is 0.34 nm. The SEM image of the PC  $(AB)^N AS$  with  $N = 19$  is shown in Fig. 1(b).

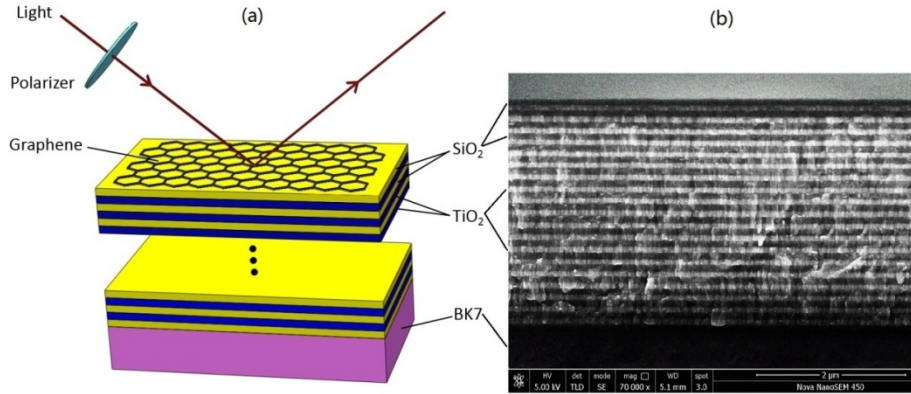


Fig. 1. (a) Schematic diagram of the composite structure,  $G(AB)^N AS$ , composed of a graphene film, G, and PC  $(AB)^N AS$  as a lossless DMM, where A denotes  $\text{SiO}_2$  with  $n_A = 1.431$  and  $d_A = 98.4$  nm, B represents  $\text{TiO}_2$  with  $n_B = 2.123$  and  $d_B = 66.4$  nm, S represents BK7 with  $n_S = 1.51$ , and N is the periodic number. (b) SEM image of the PC  $(AB)^N AS$  with  $N = 19$ .

The transfer matrix method [35] was used to calculate the transmittance ( $T$ ) and reflectance ( $R$ ) of the composite structure of  $G(AB)^N AS$ , and its absorptance ( $A$ ) was calculated using the formula  $A = 1 - T - R$ . The alternating A and B layers of the truncated PCs with the structure  $(AB)^N A$  were deposited on the planar face of the substrate (S) by an ion-assisted electron-beam evaporation under high vacuum. During the deposition, the vacuum chamber was kept at  $2.0 \times 10^{-2}$  Pa, the temperature was set at  $150^\circ\text{C}$ , Ar +  $\text{O}_2$  ion assistance with optimized oxygen partial pressure ( $1.0 \times 10^{-2}$  Pa) was applied and the ion kinetic energy of 70 eV was kept for all layers. The thicknesses of the A and B layers were monitored using quartz crystal sensors.  $T$  and  $R$  of the  $G(AB)^N AS$  sample were measured with a Cary-100 ultraviolet-visible-near-infrared spectrophotometer and an R1-angle-resolved spectrometer system.

Monolayer graphene grown via chemical vapor deposition on Cu foils was placed on the surface of the  $(AB)^N AS$  using a wet transfer method [23]. The wet transfer process was repeated to create bilayer and trilayer graphene on the top of the DMMs. The detailed process was described as follows: A poly(methyl methacrylate) (PMMA) film was spin-coated onto the graphene covered Cu foil and dried at  $170^\circ\text{C}$  for 30 min. Subsequently, a PMMA/graphene membrane was obtained by etching away the Cu foil in a  $\text{Fe}(\text{NO}_3)_3/\text{H}_2\text{O}$  solution and then transferred to the surface of the DMMs. The wet transfer process was repeated to create bilayer and trilayer graphene on the DMMs.

The reflection properties of the PC under the normal incidence of the light were studied, as shown in Fig. 2. In the forbidden gap of the PC, the truncated PC  $(AB)^N AS$  was designed to play the role of a perfect magnetic mirror with a zero reflection phase in which the values of the reflection phase [36, 37] on the surface of the  $(AB)^N AS$  are limited to between  $-\pi$  to  $\pi$ . Figures 2(a) and 2(b) provide the reflection spectra ( $R$ ) of  $(AB)^N AS$  and the reflection phase,  $\varphi_R$ , at the incident surface of  $(AB)^N AS$ , respectively. The value of the reflection phase,  $\varphi_R$ , is zero at the center wavelength ( $\lambda = 563.8$  nm) of the forbidden gap. According to the

resonance interference condition between the incident and reflection light, the total electric field intensity  $|E|^2$ , can be described as

$$|E|^2 = |E|_m^2 + |E|_r^2 + |E|_m |E|_r \cos(\phi_r) \tag{1}$$

where  $|E|_m^2$  and  $|E|_r^2$  represent the electric field intensities of the incident and reflected light, respectively. In the forbidden gap of a lossless dielectric PC,  $|E|_r^2$  equals  $|E|_m^2$ ; thus, the maximum  $|E|^2$  is four times that of  $|E|_m^2$  when  $\phi_r$  equals zero according to Eq. (1), as shown in Fig. 2(b). The reflection spectra and the reflection phase,  $\phi_r$ , of the truncated PC (BA)<sup>N</sup>BS as a perfect dielectric electric mirror (DEM) are presented in Fig. 3, where  $\phi_r$  equals  $\pi$  at the center wavelength ( $\lambda = 563.8$  nm) of the forbidden gap.

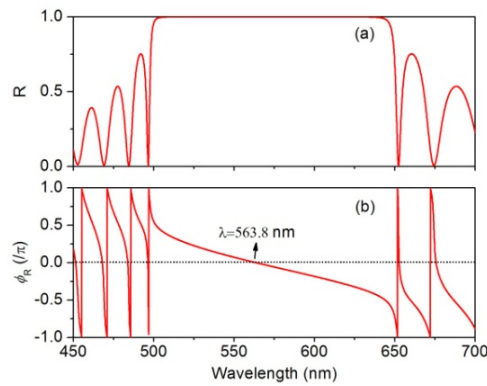


Fig. 2. Reflection spectra ( $R$ ) and reflection phase,  $\phi_r$ , of  $(AB)^{19}AS$ . At the center wavelength of  $\lambda = 563.8$  nm in the forbidden gap of PC, the reflection phase,  $\phi_r$ , of  $(AB)^{19}AS$  equals 0. Other parameters are the same as those in Fig. 1.

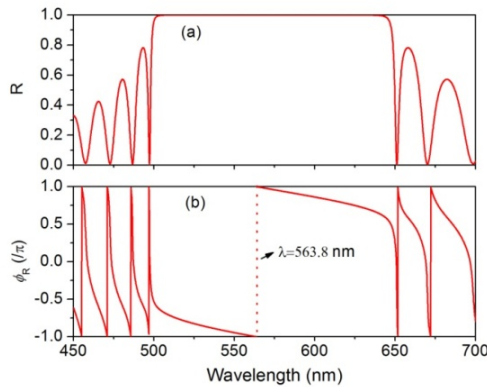


Fig. 3. Reflection spectra ( $R$ ) and reflection phase of  $(BA)^{19}BS$ . At the center wavelength of  $\lambda = 563.8$  nm in the forbidden gap of the PC, the reflection phase of  $(BA)^{19}BS$  equals  $\pi$ . Other parameters are the same as those in Fig. 2.

Figures 4(a)-4(c) show the absorption spectra ( $A$ ) of the composite structures of  $G(AB)^{19}AS$  with graphene films of different thicknesses for normal incidence, where  $G_1, G_2$

and  $G_3$  denote monolayer, bilayer and trilayer graphene, respectively. The red and blue lines describe the theoretical and experimental results, respectively. The spectra show that the absorption of the graphene films is enhanced strongly in the entire forbidden gap of the PC. The measured maximum absorptances of  $G(AB)^{19}AS$  that included monolayer, bilayer and trilayer graphene are 0.0866, 0.1692, and 0.2447 at 568.3 nm, respectively, and the corresponding simulated values at 563.8 nm are 0.0889, 0.1699, and 0.2439, respectively. The experimental spectra are in good agreement with theoretical spectra. Compared with that of the free-standing monolayer, bilayer or trilayer graphene, the absorptances of the composite structures containing graphene were enhanced by nearly four-fold.

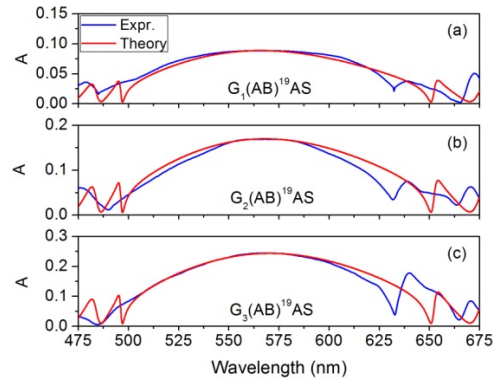


Fig. 4. Absorption spectra ( $A$ ) of the composite structure,  $G(AB)^{19}AS$ , with (a) monolayer graphene,  $G_1$ ; (b) bilayer graphene,  $G_2$ ; and (c) trilayer graphene,  $G_3$ ; for normal incidence. The red and blue lines represent the numerical and experimental results, respectively. Other parameters are the same as those in Fig. 1.

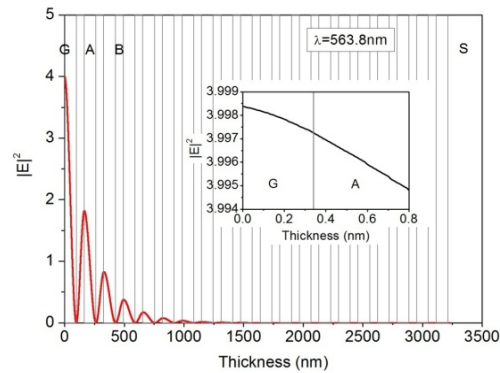


Fig. 5. Simulated electric field intensity,  $|E|^2$ , in the composite structure,  $G(AB)^{19}AS$ , at 563.8 nm and at normal incidence. The inset shows the electric field intensity in graphene of  $G(AB)^{19}AS$ . Other parameters are the same as those in Fig. 1.

To determine the physical origin of the enhanced absorption more clearly when the graphene is deposited on the surface of the truncated PC  $(AB)^N AS$ , we numerically calculated the electric field intensity distribution,  $|E|^2$ , for  $G(AB)^{19}AS$  that had the graphene monolayer at 563.8 nm, as shown in Fig. 5. The electric field intensity of the incident wave is assumed to be 1.  $|E|^2$  in the graphene monolayer was nearly four times that of the incident wave because

the PC behaves as a perfect DMM; thus, the maximum electric field intensity can be realized on the surface of the truncated PC as defined by Eq. (1). Meanwhile, the reflection phase,  $\phi_R$ , of the PC is from  $-\pi/4$  to  $\pi/4$  nearly in the entire forbidden gap and it equals zero in the center; thus, the wideband-enhanced optical absorption of graphene is realized.

For the oblique incidence of the light, absorption spectra were measured for both the transverse electric (TE) and transverse magnetic (TM) polarizations. Figures 6(a)-6(c) show the theoretical (red lines) and experimental (blue lines) absorption spectra of  $G(\text{AB})^{19}\text{AS}$  for a TE wave at a  $30^\circ$  incident angle. The enhanced absorption band of  $G(\text{AB})^{19}\text{AS}$  was broadened because the forbidden gap of the PC widened as the incident angle of the TE polarization increased. The measured maximum absorptances of  $G(\text{AB})^{19}\text{AS}$  that included the monolayer, bilayer and trilayer graphene were 0.1028, 0.1939, and 0.2733 at 540.2 nm, respectively. These values are larger than those at normal incidence. The theoretical absorptances of  $G(\text{AB})^{19}\text{AS}$  that included monolayer, bilayer and trilayer graphene at 540.2 nm were 0.1019, 0.1936, and 0.2760, respectively. Thus, the experimental spectra are consistent with the theoretical spectra. Compared with that of free-standing graphene at the same incident angle, the absorptance of  $G(\text{AB})^{19}\text{AS}$  containing the monolayer, bilayer or trilayer graphene was still enhanced by nearly four-fold. The physical origin of the enhanced absorption in the graphene-DMM at the  $30^\circ$  incident angle is similar to that at normal incidence. Figures 6 (d)-6(f) show the theoretical (red lines) and experimental (blue lines) absorption spectra of the composite structures of  $G(\text{AB})^{19}\text{AS}$  for a TM wave at a  $30^\circ$  incident angle. In contrast to those for TE polarization, the enhancement of the absorption band of  $G(\text{AB})^{19}\text{AS}$  was smaller than that at normal incidence because the forbidden gap of the PC narrowed as the incident angle of TM polarization increased. The experimental maximum absorptances of  $G(\text{AB})^{19}\text{AS}$  that included monolayer, bilayer and trilayer graphene were 0.0772, 0.1488, and 0.2158 at 548.5 nm, respectively. The calculated absorptances of  $G(\text{AB})^{19}\text{AS}$  with monolayer, bilayer and trilayer graphene at 548.5 nm were 0.0774, 0.1489, and 0.2150, respectively. The absorptance of  $G(\text{AB})^{19}\text{AS}$  was enhanced by nearly four-fold compared with that of free-standing graphene at the same incident angle.

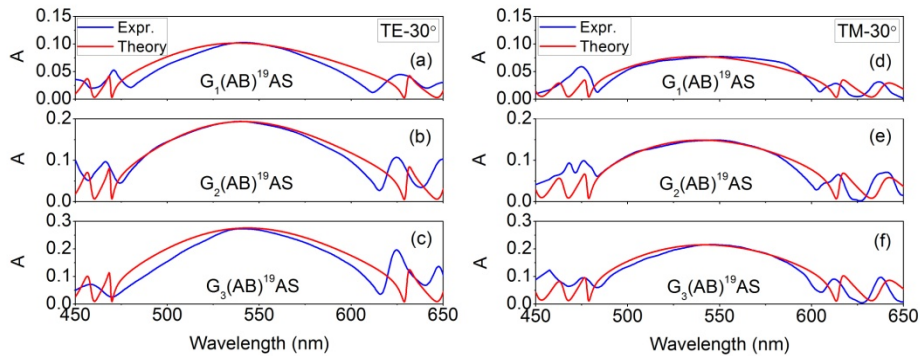


Fig. 6. Simulated (red lines) and measured (blue lines) absorption spectra ( $A$ ) of  $G(\text{AB})^{19}\text{AS}$  as a function of wavelength at an incident angle of  $30^\circ$ : (a)-(c) for a TE wave and (d)-(f) for a TM wave. Other parameters are the same as those in Figs. 1 and 5.

The above theoretical and experimental results demonstrate that the bandwidth of the enhanced absorption of the graphene on the PC is proportional to that of the forbidden gap of the PC. This finding indicates that if an omnidirectional and ultra-wide photonic forbidden gap with 0 reflection phase is realized, an omnidirectional or ultra-wide enhanced absorption band for graphene will be achieved. These properties are important to fabricate graphene-based broadband optoelectronic devices.

## 2.2 Enhancement of photocurrents in graphene on the DMM

Although graphene is considered to be a potential candidate for ultrafast optoelectronics devices [16], limitations such as low signal-to-noise ratio remain due to the weak light-graphene interaction. In this study, by utilizing a graphene-DMM heterostructure in which the DMM is realized by a truncated all-dielectric PC, enhancements of the photocurrents in graphene-based devices are achieved.

In the experiment, Cr/Au electrodes (source and drain) were deposited on the graphene layer to measure the photocurrents. By raster scanning the focused laser light with a 550 nm wavelength near the interface of graphene and the electrode, a spatial map of the photocurrent intensity was recorded, as shown in Fig. 7. At the graphene-electrode interface, photo excited electron-hole pairs in graphene could be separated by the internal electric field, forming photocurrents. To verify the enhancement of photocurrents in the graphene-DMM heterostructure, we also measured photocurrent mapping on the silica/silicon substrate for comparison. Figures 7(b) and 7(c) show that the photocurrents in the graphene-DMM heterostructure were significantly larger than that in graphene on silica/silicon substrate.

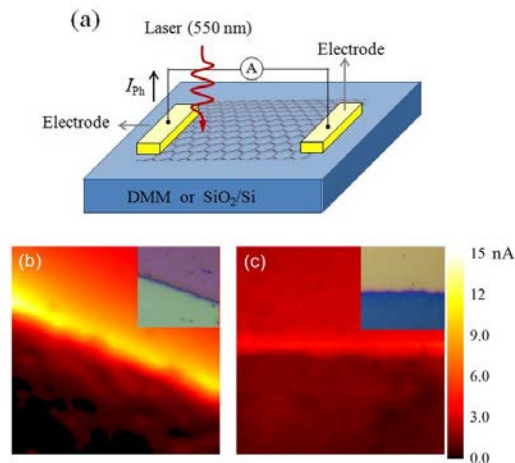


Fig. 7. (a) Schematic of the experimental setup of the photocurrent measurements, where the inset shows the optical micrograph of the interface of graphene and the electrode. Intensity map of the photocurrents in the graphene monolayer on the DMM (b) and on the silica/silicon substrate (c) at a size of  $20\ \mu\text{m} \times 20\ \mu\text{m}$ . Other parameters are the same as those in Fig. 1.

## 2.3 Enhanced Raman scattering and THG of graphene on the DMM

Raman spectroscopy is an important tool that is used to analyze the properties of graphene, such as the determination of layer numbers, defects, doping, and other variables [6, 7, 19, 38–41]. Although a Raman spectrum is readily observable from graphene, a larger signal intensity is often needed to provide a quantitative analysis of the changes in graphene properties that can occur due to external parameters, e.g., electronic doping and adsorption of gas molecules [6,7]. DMM offers an effective method to enhance the local electric field, thus providing a stronger Raman scattering of the incoming light.

Figure 8(a) shows the Raman G-mode spectra of graphene on  $\text{SiO}_2$  and DMM for an excitation laser wavelength of 632.8 nm. The excitation wavelength is out of the measured photonic band gap of DMM, and no clear difference was observed in the two cases. However, the green laser (532.0 nm) was located within the forbidden gap of the PC (AB)<sup>19</sup>AS. Accordingly, the Raman scattering is expected to increase if the green laser is employed. The results of the G-mode ( $1580\ \text{cm}^{-1}$ ) and 2D-mode ( $2670\ \text{cm}^{-1}$ ) of graphene are presented in Figs. 8(b) and 8(c), respectively. In both cases, the Raman signals increased  $\sim 5$ -fold. The

designed enhancement of the local field was 3.4-fold at 532.0 nm, whereas the radiated Raman signal also benefited from the DMM coating. As a result, the total yield for the Raman signal was larger than 3.4. Of note, the Raman wavelength is close to the red tail of the photonic band gap. The radiation Raman signal can be further enhanced by designing a DMM coating that is optimized at both the excitation and radiation wavelengths.

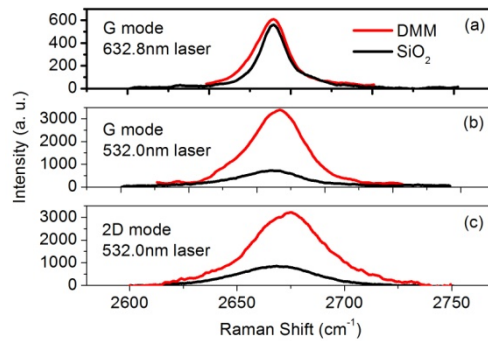


Fig. 8. Raman spectra of the monolayer graphene on  $\text{SiO}_2$  substrate (black line) and on the DMM (red line). (a) The G peak of graphene on two different substrates at an excitation laser wavelength of 632.8 nm. (b) and (c) The G peak and 2D peak of graphene on two different substrates at an excitation laser wavelength 532.0 nm, respectively. Other parameters are the same as those in Fig. 1.

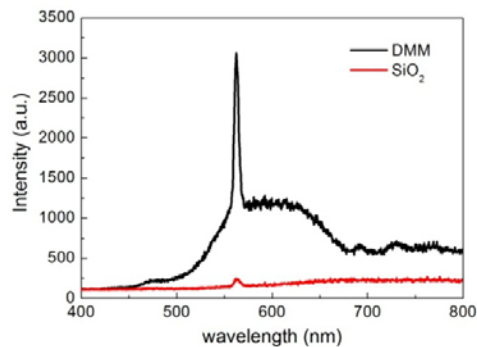


Fig. 9. THG from the monolayer graphene on DMM (black line) and on fused silica substrate (red line), respectively. The THG emerged at 563.0 nm with the femtosecond excitation laser beam at 1689.0 nm. The broad nonlinear photoluminescence [40] from monolayer graphene was also enhanced in the forbidden gap of PC.

Utilizing the strong local electric field enhancement, nonlinear optical effect of graphene can be measured with a lower excitation energy [13, 14]. To demonstrate this application, we performed a THG measurement. Figure 9 shows the data from monolayer graphene on a transparent fused silica substrate (red line) and on the DMM (black line), respectively. In the THG measurement, a linearly polarized femtosecond laser at the wavelength of 1689.0 nm was used as the excitation source, so that the wavelength of THG signal lies in the enhanced spectral range of DMM. The laser at the power of  $\sim 0.81$  mW was focused to the sample by a 100x Nikon objective (NA 0.95) and the back-scattered THG signal was collected by the same objective, and guided to a spectrograph equipped with a liquid nitrogen cooled CCD detector to acquire spectrum after short-pass filters. It can be seen that the enhanced THG from graphene on the DMM is about 14 times larger than that on the fused silica substrate. The magnification is close to the square of the designed enhancement of the local field (16

times) at 563.0 nm. As showed in Fig. 9, the broad nonlinear photoluminescence [42] from monolayer graphene was also enhanced in the forbidden gap of PC. Such results show that the nonlinear responses such as THG and nonlinear photoluminescence [42] from monolayer graphene could be dramatically enhanced by placing it on the surface of DMM.

### 3. Conclusions

We studied the enhanced interaction of light with graphene on truncated dielectric PCs, where the PCs serve as perfect DMMs. The bandwidth of the enhanced absorption of graphene was determined by the width of the forbidden gap of the PC. The local electric field enhancement was also investigated for normal and oblique incidences for both TE and TM polarizations. Our experimental results show that the maximum absorptance of graphene/DMM in the forbidden gap is nearly four times that of free-standing graphene, which agrees well with the theoretical values. Applications of this designed DMM have been demonstrated with a promising effect on photocurrents, surface Raman scattering and the nonlinear optical response of graphene. These results offer a facile solution for new compact graphene-based nanophotonic and optoelectronic devices.

### Funding

973 Program (Grants 2015CB659400, 2013CB632701); National Natural Science Foundation of China (Nos. 11264003, 11404064); Natural Science Foundation of Shandong Province (No. ZR2015AM008); open project of State Key Laboratory of Surface Physics and Department of Physics (No. KF2017\_01), open projects of Key Laboratory of Micro- and Nano-Photonic Structures (Ministry of Education) and State Key Laboratory of Surface Physics (Nos. ZA2014-01, KF2015-04).

### Acknowledgment

L. S. appreciates the support from National 1000 Youth Talent Project of China and the Professor of Special Appointment (Eastern Scholar) at Shanghai Institutions of Higher Learning.